| | |
|---|---|
| Title | Synergistic capacitive behavior between polyaniline and carbon black |
| Author(s) | Wang, Huanhuan; Liu, Jilei; Chen, Zhen; Chen, Shi; Sum, Tze Chien; Lin, Jianyi; Shen, Ze Xiang |
| Citation | Wang, H., Liu, J., Chen, Z., Chen, S., Sum, T. C., Lin, J., et al. (2017). Synergistic capacitive behavior between polyaniline and carbon black. Electrochimica Acta, 230, 236-244. |
| Date | 2017 |
| URL | http://hdl.handle.net/10220/43509 |
| Rights | © 2017 Elsevier. This is the author created version of a work that has been peer reviewed and accepted for publication by Electrochimica Acta, Elsevier. It incorporates referee's comments but changes resulting from the publishing process, such as copyediting, structural formatting, may not be reflected in this document. The published version is available at: [http://dx.doi.org/10.1016/j.electacta.2017.01.164]. |

# Synergistic capacitive behavior between polyaniline and carbon black

**Huanhuan Wang,[a,b] Jilei Liu,[c,d*] Zhen Chen,[c,d] Shi Chen,[c] Tze Chien Sum,[c] Jianyi Lin[d*] and Ze Xiang Shen[c,a,b*]**

[a] CINTRA CNRS/NTU/Thales, UMI 3288, 50 Nanyang Drive, 637553, Singapore.

[b] School of Materials Science and Engineering, Nanyang Technological University, 50 Nanyang Avenue, 639798, Singapore.

[c] Division of Physics and Applied Physics, School of Physical and Mathematical Sciences, Nanyang Technological University, 21 Nanyang Link, 637371, Singapore.

[d] Energy Research Institute (ERI@N), Interdisciplinary Graduate School, Nanyang Technological University, Research Techno Plaza, 50 Nanyang Drive, 637553, Singapore.

*Authors to whom correspondence should be addressed: Tel: (65) 6316 2975. E-mail: Liujilei036@163.com (Liu Jilei); Tel: (65) 6316 8855. E-mail: LiJY@ntu.edu.sg (Lin Jianyi); Tel: (65) 9712 5670. E-mail: Zexiang@ntu.edu.sg (Shen Ze Xiang)

## Graphical abstract

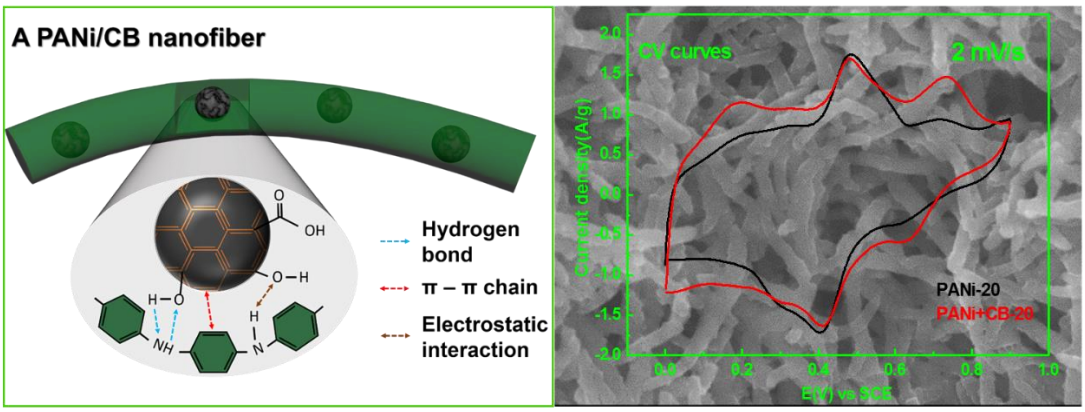

**Abstract**

Polyaniline (PANi) is an excellent electrode material with high pseudocapacitance for supercapacitors. Here the binder-free supercapacitor electrodes with high specific capacitance (458 F $g^{-1}$ at 2 mV $s^{-1}$) and Coulombic efficiency (100%) are successfully synthesized via a one-step potentialdynamic co-deposition of PANi and carbon black (CB). Significant synergistic effect between PANi and CB is demonstrated. Particularly, CB as the secondary dopant of PANi has been found to play an important role in producing higher conductivity, extended conformation structure, improved porosity, higher oxidation state and depressed hydrolysis effect, leading to superior capacitive performance. This promotes better understanding about synergistic effect between active materials and carbon additives, and opens up new research and direction for high performance electrode design.

**Keywords**

Synergistic effect; supercapacitor; PANi; CB

## 1. Introduction

Supercapacitors with high power density, long-term cycling stability and high reversibility have been rising as promising energy storage devices. There are three main types of electrode materials for supercapacitors, namely, carbon species, metal compounds and conducting polymers [1-4]. The combination of carbonaceous materials, metal compounds and conducting polymers in a composite system usually results in improved performance due to the synergistic effect of every component [5, 6].

Polyaniline (PANi) has been extensively studied as electrode materials for supercapacitors for its excellent properties, including high pseudocapacitance, high conductivity, high flexibility and low cost [7-9]. The excellent capacitive properties and fast charge transfer usually result in high energy/power density and good rate capability for supercapacitors. Moreover, the flexibility makes PANi promising to fabricate flexible electrodes. However, the pseudocapacitance of PANi is not always high and its capacitive behaviors is significantly dependent on its structural and chemical properties [3, 10]. PANi can exist in three different oxidation states: fully reduced leucoemeraldine (LE), 50%-oxidized emeraldine base (EB) and

fully oxidized pernigraniline (PE). EB is the most stable form of PANi, consisting of equal numbers of reduced amine (–NH–) and oxidized imine (–N=) units [11], as shown in Fig. 1a. Upon doping with acid, neutral EB, which is insulating with a wide band gap can be converted to protonated emeraldine salt (ES), which is electrically conducting. LE and PE are insulators, even when doped. PANi-ES with reduced amine and oxidized imine units possesses an asymmetric electronic structure in the energy band gap [12], where the protonation of imine (–N=) sites and the subsequent internal redox reaction induce two asymmetric polaron bands. The upper polaron band (p*) is narrow and nearly degenerated in the conduction band while the lower band (p) is broad. Hence the protonation results in the shift of Fermi level from the middle of the band gap to the middle of the half-occupied lower polaron band (as schematically shown in Fig. 1b). The polaron bands facilitate the electron transition across the band gap, resulting in significantly enhanced conductivity of PANi-ES [13]. When PANi-EB is protonated, the polymer backbone is positively charged and the negative counterions like $SO4^{2-}$ could sit in the vicinity of polymer chains, resulting in the so-called PANi-ES. It will cause the change of the conformation, conjugation length of PANi, which are significantly related to the conductivity, as well as the electrochemical performance.

Even the conductivity of PANi could be greatly increased by the doping of acid that increases the electrochemical performance, the inferior mechanical stability due to swelling, shrinkage or crack and the degradation due to side reactions during the polymerization and electrochemical test will restrict its application in supercapacitors. As mentioned above, PANi has three different forms based on the oxidation states. Besides, there are also unwanted side products like p-benzoquinone (BQ) and hydroquinone (HQ) due to the hydrolysis. The hydrolysis is unavoidable during the polymerization, which will affect the conductivity, reversibility and stability of PANi [14, 15].

Carbon materials are common supercapacitor materials with high stability but low specific capacitance[16, 17]. Recently, many PANi based composites containing nanostructured carbon materials such as carbon nanotubes (CNTs), graphene and various porous carbon materials have been reported with enhance electrochemical performance for supercapacitors. The presence of nanostructured carbonaceous materials in hybrid PANi/C electrodes can significantly enhance the stability, conductivity and the dispersibility of PANi, resulting in enhanced electrochemical performance. Graphene and CNTs are popularly used in energy storage and show excellent intrinsic electronic, structural and mechanical properties [18, 19]. Many investigations have been conducted on PANi based composite electrodes involving

graphene or CNTs, which show high specific capacitance over 500 F $g^{-1}$ and good cycling stability of around 90% capacity retention after hundreds of electrochemical cycles [7-9, 20-22]. However, the syntheses of graphene normally follow the Hummer's method with complicated chemical process [8]. The resulting graphene oxide (GO) suffers from low conductivity, which needs to be reduced to reduced graphene oxide (rGO). Several works focused on functional-rGO (frGO), such as nitrophenyl-rGO and aminophenyl-rGO, which were found to further enhance the performance of PANi/frGO [8]. Besides, CNTs are usually obtained through the chemical vapor deposition and surfactant of dopant is introduced to modify the surface properties of CNTs to facilitate the combination with PANi [20]. Most of these works were time consuming or cost ineffective due to complicated chemical process and prohibitive cost of graphene and CNTs, which could hamper the commercial application.

In this paper, we adopt a facile electrochemical co-deposition method to achieve freestanding PANi/CB electrode on porous graphite substrates, using low cost precursors. The potentialdynamic polymerization is employed because it can produce binder-free electrode with uniform porous-network in short reaction time with a simple set-up (Fig. 2a), and allow a fine-tuning of mass loading of active materials. The hybrid composites exhibit improved electrochemical performance due to the addition of CB in terms of specific capacitance (458 F $g^{-1}$, 2 mV $s^{-1}$), cycling stability (74% retention after 300 cycles) and Coulombic efficiency (100%), which are among the best results in literature on PANi and commercial active carbon materials [23-29], while the pure PANi only delivers a specific capacitance of 381 F $g^{-1}$ with 70% retention after 300 cycles and 74% Coulombic efficiency. This is attributed to the significant synergistic effect between PANi and CB. Particularly, several roles of CB have been identified: (i) It promotes the formation of extended PANi chains to be much thinner, longer and more porous than pure PANi. This extended conformation is favorable for electron transfer and ion diffusion, thus enhancing the electric conductivity and ensuring high capacity resulting from more active sites exposed to the electrolyte. (ii) The CB nanoparticles can be well-wrapped in PANi chains without inducing any additional resistance. (iii) It can increase the doping level and decrease the defects density of PANi, facilitating the transfer of bipolarons to polarons and delocalization of polarons and ensuring the improved electric conductivity [3]. All these contribute to the enhanced electrochemical performance.

## 2. Experimental

### 2.1 Fabrication of PANi/CB Composite Electrode

The electrochemical co-deposition was carried out on the EC workstation (CHI 760D) with a three-electrode system, where graphite paper (GP), a Pt sheet and a saturated calomel electrode (SCE) acted as the working electrode (WE), counter electrode (CE) and reference electrode (RE), respectively. Fresh distilled aniline ($C_6H_5NH_2$) and vulcan XC-72 carbon black with the concentration of 0.1 mol $dm^{-3}$ and 1 g $dm^{-3}$ respectively were dispersed in 0.5 mol $dm^{-3}$ $H_2SO_4$ as the deposition electrolyte. The potentialdynamic deposition was cycled between -0.2 and 0.8 V under a stirring speed of 300 rpm to guarantee homogenous growth. Different scan rates of 10, 20 and 50 mV $s^{-1}$ were involved and the samples were denoted as PANi+CB-10, PANi+CB-20 and PANi+CB-50, respectively. For comparison, the control samples of PANi were also prepared in a 0.5 mol $dm^{-3}$ $H_2SO_4$ containing 0.1 mol $dm^{-3}$ aniline without CB named as PANi-10, PANi-20 and PANi-50, respectively. In order to study the effects of substrates, the GP was also replaced by stainless steel (SS) and the resultant electrodes obtained at 20 mV $s^{-1}$ was named as PANi+CB-20-SS. All electrodes were washed with deionized water to remove the residual reactants and sulfuric acid. The loading mass of active materials (Table S2) was determined by weighing of the dry and clean working electrodes before and after the electrochemical polymerization.

**2.2 Structural and spectroscopic Analyses**

Field Emission Scanning Electron Microscope (FE-SEM) (Model Jeol JSM 6700F) and Transmission Electron Microscope (JEM-2010F, TEM, acceleration voltage: 200 kW) were employed to study the morphology of the samples. Structural and bonding information were obtained by Fourier Transform Infrared Spectroscopy (FTIR), Raman spectroscopy and UV-visible spectroscopy that were performed on PerkinElmer Spectrum GX, Renishaw (laser wavelength: 532 nm), and SHIMADZU UV-2700, respectively. The surface chemical states were examined by X-ray Photoelectron Spectroscopy (XPS, SPECS), with a VG ESCALAB 220i-XL system using a monochromatic Al Kα photon source (hν=1486.7eV). The nitrogen adsorption and desorption isotherms were obtained by Quantachrome Instruments Autosorb-iQ (Boynton Beach, Florida USA).

**2.3 Electrochemical Characterization**

The electrochemical properties of as obtained green-colored PANi on substrates were studied on a CHI760D Electrochemical workstation (CHENHUA, Shanghai, China) to study the electrochemical properties. The cyclic voltammetry (CV) and galvanostatic charge-

discharge were both conducted in the potential range from 0 to 0.9 V with the scan rates of 2 to 20 mV $s^{-1}$ and current densities of 0.1 to 5 A $g^{-1}$, respectively. The electrochemical impedance spectroscopy (EIS) characterization was performed in the frequency range of 100 kHz to 0.01Hz for the samples. All tests were conducted in 0.5 M $H_2SO_4$ electrolyte.

**3. Results and discussions**

SEM images shown in Fig. 2b and Fig. 2c reveal the nanofibrous structure of PANi samples. For PANi+CB-20, the PANi fibers exhibit diameter of 50-80 nm with length in the range of 1-2 μm, which is much longer and thinner than those (100-120 nm in diameter and ~1 μm in length) of PANi-20, indicating that the presence of CB can facilitate the growth of long and thin PANi nanofibers. This larger aspect ratio (L/D) for PANi+CB-20 is in good agreement with previous studies that the addition of carbonous dopants or other additives could change the conformation and form extended chains of PANi by removing twist defects in the aromatic rings in PANi [30]. The extended feature is advantageous for enhancing the electronic conductivity due to the stronger interaction between adjacent bipolarons and the delocalization of polarons (see Fig. 1a), and ensuring high capacity resulting from more active sites exposed to the electrolyte.

As shown in the TEM images, the spherical CB nanopaticles are well wrapped in the single stranded PANi nanofibers uniformly (Figs. 2d, 2e). The intact electronic/physical contact between CB and PANi is favorable for electron transfer and ion diffusion, thus yielding high specific capacitance. This is further verified by $N_2$ adsorption and desorption results in Fig. 2f, the negligible change of specific surface area (SSA) for two samples indicates CB well-encapsulated in the PANi chains. In Fig. 2g, PANi+CB-20 exhibits more mesoporous sized at 3.0 nm and 4.5 nm than PANi-20. This pore size distribution feature is particularly favorable for supercapacitors.

The morphology of PANi/CB depends both on the scan rate and substrate of potentialdynamic deposition. As shown in Figure. S2a and b, PANi+CB-10 is composed of short nanorods while PANi+CB-50 mainly contains entangled and merged nanofibers, giving rise to a compact structure. These results are consistent with previous studies. The growth of PANi nanofibers through electrochemical deposition involves the horizontal growth of a compact nucleation layer and the following vertical growth of PANi nanofibers [31]. The amount of PANi nuclei is proportional to the deposition scan rates [32]. At lower scan rates,

the oxidation time is longer for the growth of PANi on less amount of nuclei, thus achieving shorter nanorods with larger horizontal dimensions. Higher scan rate is favorable for more PANi nuclei, so the nanofibers of PANi+CB-50 are much more compact compared with PANi+CB-10 and PANi+CB-20. In addition, the morphology of PANi is strongly dependent on substrate type. For PANi+CB-20-SS (Fig. S2c), the electrode materials consist of large-sized nanoparticles with large mesopores (average pore size around 8nm) and limited nanopores. The low specific surface area (19.491 $m^2/g$) and low pore volume (Figs. S1c, S1d) impede the ion diffusion in the electrode, which emphasizes the great effect of substrates in electrochemical polymerization of PANi. On the contrary, GP with higher porosity and larger surface area could promote vertical growth of PANi due to the good dispersibility of PANi nuclei on the surface of substrate, resulting in larger quantity and better structured PANi nanofibers [33].

The FTIR, Raman and UV-visible spectra of PANi based samples are shown in Fig. 3. The IR bands around 1105 $cm^{-1}$, 1240 $cm^{-1}$ and 1300 $cm^{-1}$ in the PANi-20 spectrum are assigned to the quinoid Q=N stretching vibrations (Q represents of quinoid unit) [34], the $C{-}N^{\bullet+}$ stretching vibrations and the C–N amine stretching vibrations, respectively [35]. The bands centered around 815 $cm^{-1}$, 1480 $cm^{-1}$ and 1558 $cm^{-1}$ are attributed to C–H out of plane vibrations in aromatic ring deformation, C–C stretching vibration in benzene and quinone ring, respectively [35]. Similar peaks are identified for PANi+CB-20. However, the peak intensity is much weaker for PANi+CB-20 due to the presence of CB. The broad band around 3420 $cm^{-1}$ and narrow band at 2912 $cm^{-1}$, which are respectively attributed to O–H and C–H stretching vibration in CB, disappear in PANi+CB-20 spectrum, corroborating the covalent interaction between CB and PANi via functional groups [36]. These interactions may include the hydrogen bonding between O–H/C–O groups of CB and –NH– sites of PANi as schematically illustrated in Fig. 3b. Moreover, the π–π stacking between the aromatic rings of CB and PANi may also exist [37]. These interactions can not only stabilize the structure of the composite, but also improve the PANi backbone chain conformation, facilitating the transfer of bipolarons to polarons and the delocalization of polarons (refer to Fig. 1a).

In Fig. 3c, the Raman spectra of XC-72 CB show a D band at 1343 $cm^{-1}$ and a G band at 1594 $cm^{-1}$, which represent the breathing modes of rings due to the defects and the in-plane stretching motion of C-C bond in carbon black [34], and remain observable in PANi and PANi/CB spectra. For PANi-20, the peaks at 810, 1170, 1332, 1479 and 1598 $cm^{-1}$ are

attributed to the out of plane C-H motions, in-plane bending of C–H in semi-quinoid (SQ) units, $C–N^{\bullet+}$ stretching, N=Q=N stretching in quinonoid rings and C=C stretching in the SQ rings, respectively [34, 35]. These Raman peaks are characteristic of PANi and also observed in the PANi+CB-20 spectrum. Nevertheless, the peak intensity at 1170 and 1479 $cm^{-1}$ is much stronger for PANi+CB-20 than that of PANi-20, indicating more imine sites connected with quinonid rings due to the presence of CB, which corresponds to the enhanced bipolaron/polaron formation and hence the enhanced conductivity for PANi+CB-20 as compared with PANi-20 (refer to Fig. 1a). These effects can be further verified by UV-visible measurements. In Fig. 3d, the UV-visible band at 360 nm and 454 nm for PANi-20 are attributed to the transition between the valance band to the conduction band ($\pi$-$\pi^*$) of benzenoid rings and the lower polaron band to conduction band (p-$\pi^*$), respectively (refer to Fig. 1b) [37, 38]. CB shows maximum adsorption at 265 nm, which is attribute to the aromatic $\pi$-$\pi^*$ transition of C-C bonds. In the case of the PANi+CB-20, the shoulder around 240 nm is blue-shifted compared with the spectrum of pure CB, which could be a result of interactions between PANi and CB. Moreover, the p-$\pi^*$ transition band shifts from 454 nm to 460 nm for PANi+CB-20. This red shift corresponds to the decrease of the gap energy between the lower polaron band (p) and the conduction band, from 2.73 eV to 2.69 eV. Moreover, the PANi+CB-20 spectrum shows a higher upward tendency above 600 nm, which is attributed to the excitation of valence electrons to the lower polaron band (p). This substantial enhancement of excitation in high wavelength range suggests the abundant delocalized polarons with the presence of CB [39]. As the transition of valence band to polaron band and polaron to conduction band are tremendously facilitated for PANi+CB-20, the transition between valence band and conduction band is negligible with the absence of absorption peak around 360 nm.

XPS analysis was conducted to shed more light on element information of PANi based electrodes. The S, C, N and O elements are identified for PANi-20 and PANi-CB-20 (Fig. S3). Sulfur comes from the doping of $SO_4^{2-}$ during the polymerization process [40]. The atomic ratio of C to N is around 6 for PANi-20 (Table S1), which agrees well with the ratio for pristine PANi where each benzene/quinoid ring is connected to one N atom (either in amine or in imine). The much higher C to N ratio in PANi+CB-20 indicates the successful addition of CB in PANi+CB-20. The C 1s spectra of PANi-20 and PANi+CB-20 can both be fitted into four sub-peaks at 283.9 eV (C=C), 284.6 eV (C–C/C–H), 285.5 eV (C–O) and 286.9 eV (C=O), respectively (Figs. 4a, 4c). The peak of C-C bond with a binding energy of 284.6 eV acts as the reference. The substantial increase of C=C peak intensity for PANi+CB-20 is due to the

presence of CB, corresponding to the higher degree of oxidation and thus higher conductivity of PANi with the addition of CB. In the same spectra, the reduction in the C-O peak intensity at 285.5 eV (0.17 for PANi+CB-20 vs. 0.41 in PANi-20) appears to mean a lower defect density due to the incorporation of carbon particles. The XPS N 1s core-level spectra in Fig. 4b and Fig. 4d are deconvolved into four Gaussian–Lorentzian sub-peaks centered at 398.2 eV (=N–), 399.0 eV (–NH–), 400.1 eV ($–N^+H–$), 401.6 eV ($=N^+H–$), respectively. Similarly, the ratio of imine to amine, i.e. [=N–]/[–NH–] is indicative of the oxidation/polymeric level of PANi chain [41]. The value is 0.23 for PANi+CB-20, larger than the value of 0.16 for PANi-20, corresponding to a higher polymeric level in PANi+CB-20 [38, 41]. These results are coherent with FTIR, Raman and UV-visible results, corroborating the higher oxidation level and enhanced electronic properties with the presence of CB.

Electrochemical properties of PANi based electrodes were investigated in a three-electrode system containing 0.5 M $H_2SO_4$ solution. Typical cyclic voltammetry curves for PANi+CB-20 and PANi-20 are shown in Fig. 5a. The CV curve of the PANi+CB-20 exhibits much larger area than that of PANi-20, indicating that the addition of CB is favorable for the enhancement of specific capacitance. Three redox pairs have been identified in the CV curves of PANi+CB-20. The first redox pair ($O_1/R_1$ ~ 0.2V) is attributed to the transition between semiconducting leucoemeraldine (LE) form and the conducting polaronic emeraldine salt (ES), the second one ($O_2/R_2$ ~ 0.45V) is corresponding to the transition between p-benzoquinone (BQ) and hydroquinone (HQ). The BQ produced during the polymerization of PANi is a side product of the hydrolysis [15]. The third one ($O_3/R_3$ ~ 0.75V) represents the transition between ES state and the fully oxidized (per) nigraniline (PE), respectively [42, 43]. For PANi-20, the first and third pairs of redox peaks are substantially suppressed (almost negligible) because of the excessive formation of BQ. Although BQ and HQ as the side-products from hydrolysis can still contribute to the specific capacitance, they may affect the electronic properties of PANi and the stability of the electrode [14, 44]. Interestingly, the second redox pair (BQ/HQ) is depressed in PANi+CB-20 compared with that of PANi-20 and hence can enhance the conductivity and stability of the composite. This is probably because the attachment of CB nanoparticles partially protects the active sites (–NH–) in PANi from being attacked by water.

Besides the protective effect of the dopant (CB), the hydrolysis was found to be affected by the morphology of PANi. As shown in Fig. S4, PANi+CB-10 and PANi+CB-50 both show high intensity of BQ/HQ. For PANi+CB-10, short nanorods mainly consist of short PANi

chains, which can be easily attacked by water, leading to high hydrolysis effect. As for PANi+CB-50, higher scan rate means the reduced oxidation time and thus hydrolysis effect is promoted since the chain growth and hydrolysis of PANi are competing to each other [15, 32]. The potential separation of the second pair of redox peaks for PANi+CB-50 is evidently larger than PANi+CB-10 and PANi+CB-20, indicating inferior reversibility, which results in poor rate capability as shown in Table S2.

The specific capacitance was calculated based on cyclic voltammetry (CV) curves. A specific capacitance of 458 F $g^{-1}$ is obtained for PANi+CB-20 at 2 mV $s^{-1}$, which is higher than 381 F $g^{-1}$ of pure PANi-20 and pure 90 F $g^{-1}$ of CB (see Fig. 5a and Fig. S5). The CV curve of CB is almost symmetric rectangle shape indicating an electrochemical double-layer capacitive properties. In order to study the effect of substrates for the electrochemical deposition of PANi, we synthesized the electrode materials with same method on stainless steel (SS) substrate and test the electrochemical performance. The CV curve for PANi+CB-20-SS in Fig. S4 is of triangular and narrow shape with much lower specific capacitance 231 F $g^{-1}$ vs. 458 F $g^{-1}$ of PANi+CB-20. This triangular shape may be caused by small effective pore size of electrode materials on SS, which inhibits the access of large anions ($SO_4^{2-}$) into the pores for double layer capacitance [45]. The low specific surface area and poor porous structure (Fig. S1) of PANi+CB-20-SS lead to less accessible surface area, which will restrain the ions adsorption and transportation, resulting in low specific capacitance [33].

The specific capacitance was also calculated based on galvanostatic discharge curves. At 0.1 A $g^{-1}$, PANi+CB-20 also shows higher capacitance of 382 F $g^{-1}$ vs. 288 F $g^{-1}$ of PANi-20 (see Fig. 5b). Furthermore, the Coulombic efficiency increases from 74% for PANi-20 to 100% for PANi+CB-20, indicating significantly enhanced reversibility. The cycling stability of PANi+CB-20 is also greatly improved by the presence of CB in the composite (Fig. 5c). PANi+CB-20 can maintain specific capacitance at 180 F $g^{-1}$ with 74% capacitance retention after 300 cycles, which is higher than that of PANi-20 (140 F $g^{-1}$ with 70% capacitance retention). Even after 650 cycles, PANi+CB-20 shows 63% capacity retention, which is comparable to those in literature for rGO-PANi composites [46]. The capacity degradation is maily due to (i) the hydrolysis effect and (ii) the structural change. The former one will result in side products with low conductivity and stability. Consequently, the specific capacity will drop, especially at high scan rates. In addition, the hydrolysis of PANi may damage the initial fiber-like structure of PANi, resulting in poor conductivity and decreased surface area. Besides

the hydrolysis, the latter one, structural change is also related with the doping and dedoping of ions in the electrolyte. All these, together, lead to sluggish electrochemical kinetics, reduced exposure surface area of active materials and poor contact between the electrode/electrolyte, and thus, a capacity fade. The capacity of PANi-20 decays in the initial cycles and then increase to the maximum at around 300 cycles (Fig. 5c). The initial capacitance fade for PANi-20 may be due to the degradation of PANi (e.g. via hydrolysis side reaction), while the increase from 200 to 300 cycles may result from the improved wettability via sufficient soaking of electrolyte during previous charge-discharge process. The results in Fig. 5c indicate that the presence of CB can improve the wettability of electrodes to the electrolyte solution and thus the electrochemical performance.

The electrochemical impedance spectra (EIS) for PANi-20 and PANi+CB-20 are compared in Fig. 5d. The slope of the Warburg tail in low frequency region is smaller than 45$^{o}$ from horizontal axis for PANi-20 while the PANi+CB-20 electrode exhibits an almost vertical straight line, which reveals faster Warburg ion diffusion and better capacitive behavior in PANi+CB-20. The lower ion diffusion resistance can be correlated to the larger aspect ratio of polymer chains measured by SEM in Fig. 2, which is in favor to the ion diffusion from the electrolyte to the pore structure of the PANi/CB composites [47, 48]. In the high-frequency region, the equivalent series resistance (ESR) and charge transfer resistance (Rct) are estimated to be ESR=1.5 Ω, 2 Ω and Rct=1.5 Ω, 6.4 Ω for PANi+CB-20 and PANi-20, respectively.

The enhanced electric conductivity as well as the improved specific capacitance and cycling stability are attributed to the addition of CB: (i) It has improved the conformation structure to form extended chains, resulting in longer and thinner PANi fibers with more mesopores of 3.0 -4.5 nm. This confirmative structure provides more active sites exposed to the electrolyte. (ii) CB is embedded in PANi fibers with intact contact. The presence of CB as the second dopant in PANi promotes the formation and delocalization of polarons, substantially improving the conductivity. (iii) The doping of CB increases the polymeric level, suppresses hydrolysis side reaction, and decreases the defects density. All these contribute to higher specific capacitance, better reversibility and longer cycle life.

## 4. Conclusions

The binder-free supercapacitor electrodes with high specific capacitance (458 F $g^{-1}$), good cycling stability (74% retention after 300 cycles) and high coloumbic efficiency (100%), are

designed based on PANi and CB composites. Significant synergistic effect between PANi and CB is demonstrated. The addition of CB is found: (i) to promote the formation of extended PANi chains that are much thinner, longer and more porous than CB-free PANi, (ii) to ensure better wettability of PANi to the electrolyte and thus better electrochemical contact, and (iii) to induce higher doping level of PANi, facilitating the transfer of bipolarons to polarons and delocalization of polarons and thus ensuring the improved electric conductivity and capacity. In addition, the facile synthesis method adopted here is superior over conventional chemical synthesis route in terms of simpler procedure, lower cost and improved performance. It can also be expanded to many other fields such as anticorrosion [49], rechargeable batteries [50], electrochemical energy conversion [41] and capacitive de-ionization(CDI) for water purification [51], where PANi based systems have attracted increased attention. This displays great practical significance of our facile work.

## Acknowledgements

The authors acknowledge financial support from the CNRS International NTU THALES Research Alliance (CINTRA), NTU, Singapore. We also acknowledge the financial support from the Ministry of Education, Tier 1 (Grant no:M4011424.110) and Tier 2 (Grant no: M4020284.110).

## Appendix A. Supplementary data

Supplementary data related to this article can be found at http://.....

Reference

[1] H. Jiang, J. Ma, C.Z. Li, Mesoporous Carbon Incorporated Metal Oxide Nanomaterials as Supercapacitor Electrodes, Adv. Mater. 24 (2012) 4197.
[2] L.L. Zhang, X.S. Zhao, Carbon-based materials as supercapacitor electrodes, Chem. Soc. Rev. 38 (2009) 2520.
[3] G.A. Snook, P. Kao, A.S. Best, Conducting-polymer-based supercapacitor devices and electrodes, J. Power Sources 196 (2011) 1.
[4] R.R. Salunkhe, Y.V. Kaneti, J. Kim, J.H. Kim, Y. Yamauchi, Nanoarchitectures for Metal–Organic Framework-Derived Nanoporous Carbons toward Supercapacitor Applications, Acc. Chem. Res. 49 (2016) 2796.
[5] J.L. Liu, L.L. Zhang, H.B. Wu, J.Y. Lin, Z.X. Shen, X.W. Lou, High-performance flexible asymmetric supercapacitors based on a new graphene foam/carbon nanotube hybrid film, Energy Environ. Sci. 7 (2014) 3709.
[6] R.R. Salunkhe, J. Tang, N. Kobayashi, J. Kim, Y. Ide, S. Tominaka, J.H. Kim, Y. Yamauchi, Ultrahigh performance supercapacitors utilizing core-shell nanoarchitectures from a metal-organic framework-derived nanoporous carbon and a conducting polymer, Chem. Sci. 7 (2016) 5704.

[7] G.Q. Ning, T.Y. Li, J. Yan, C.G. Xu, T. Wei, Z.J. Fan, Three-dimensional hybrid materials of fish scale-like polyaniline nanosheet arrays on graphene oxide and carbon nanotube for high-performance ultracapacitors, Carbon 54 (2013) 241.
[8] L.F. Lai, H.P. Yang, L. Wang, B.K. Teh, J.Q. Zhong, H. Chou, L.W. Chen, W. Chen, Z.X. Shen, R.S. Ruoff, J.Y. Lin, Preparation of Supercapacitor Electrodes through Selection of Graphene Surface Functionalities, ACS Nano 6 (2012) 5941.
[9] J.L. Liu, J. Sun, L.A. Gao, A Promising Way To Enhance the Electrochemical Behavior of Flexible Single-Walled Carbon Nanotube/Polyaniline Composite Films, J. Phys. Chem. C 114 (2010) 19614.
[10] K. Lota, V. Khomenko, E. Frackowiak, Capacitance properties of poly(3,4-ethylenedioxythiophene)/carbon nanotubes composites, J. Phys. Chem. Solids 65 (2004) 295.
[11] D. Li, J.X. Huang, R.B. Kaner, Polyaniline Nanofibers: A Unique Polymer Nanostructure for Versatile Applications, Accounts Chem. Res. 42 (2009) 135.
[12] J. Kim, S. Park, N.F. Scherer, Ultrafast Dynamics of Polarons in Conductive Polyaniline: Comparison of Primary and Secondary Doped Forms, J. Phys. Chem. B 112 (2008) 15576.
[13] C.H.B. Silva, N.A. Galiote, F. Huguenin, E. Teixeira-Neto, V.R.L. Constantino, M.L.A. Temperini, Spectroscopic, morphological and electrochromic characterization of layer-by-layer hybrid films of polyaniline and hexaniobate nanoscrolls, J. Mater. Chem. 22 (2012) 14052.
[14] N. Gospodinova, P. Mokreva, L. Terlemezyan, Influence of hydrolysis on the chemical polymerization of aniline, Polymer 35 (1994) 3102.
[15] C.Q. Cui, L.H. Ong, T.C. Tan, J.Y. Lee, Extent of incorporation of hydrolysis products in polyaniline films deposited by cyclic potential sweep, Electrochim. Acta 38 (1993) 1395.
[16] B.L. Xing, J.L. Cao, Y. Wang, G.Y. Yi, C.X. Zhang, L.J. Chen, G.X. Huang, B. Xu, Preparation of lignite-based activated carbon with high specific capacitance for electrochemical capacitors, Funct. Mater. Lett. 8 (2015) 1550031-1.
[17] J. Tang, Y. Yamauchi, CARBON MATERIALS MOF morphologies in control, Nat. Chem. 8 (2016) 638.
[18] A.A. Balandin, Thermal properties of graphene and nanostructured carbon materials, Nat. Mater. 10 (2011) 569.
[19] A.K. Geim, K.S. Novoselov, The rise of graphene, Nat. Mater. 6 (2007) 183.
[20] Y. Yang, Y. Hao, J. Yuan, L. Niu, F. Xia, In situ preparation of caterpillar-like polyaniline/carbon nanotube hybrids with core shell structure for high performance supercapacitors, Carbon 78 (2014) 279.
[21] J. Yan, T. Wei, Z. Fan, W. Qian, M. Zhang, X. Shen, F. Wei, Preparation of graphene nanosheet/carbon nanotube/polyaniline composite as electrode material for supercapacitors, J. Power Sources 195 (2010) 3041.
[22] R.R. Salunkhe, S.H. Hsu, K.C.W. Wu, Y. Yamauchi, Large-Scale Synthesis of Reduced Graphene Oxides with Uniformly Coated Polyaniline for Supercapacitor Applications, ChemSusChem 7 (2014) 1551.
[23] M.J. Bleda-Martinez, E. Morallon, D. Cazorla-Amoros, Polyaniline/porous carbon electrodes by chemical polymerisation: Effect of carbon surface chemistry, Electrochim. Acta 52 (2007) 4962.
[24] K.S. Ryu, Y.G. Lee, K.M. Kim, Y.J. Park, Y.S. Hong, X.L. Wu, M.G. Kang, N.G. Park, R.Y. Song, J.M. Ko, Electrochemical capacitor with chemically polymerized conducting polymer based on activated carbon as hybrid electrodes, Synth. Met. 153 (2005) 89.
[25] D. Salinas-Torres, J.M. Sieben, D. Lozano-Castello, D. Cazorla-Amoros, E. Morallon, Asymmetric hybrid capacitors based on activated carbon and activated carbon fibre-PANI electrodes, Electrochim. Acta 89 (2013) 326.
[26] W.C. Chen, T.C. Wen, H.S. Teng, Polyaniline-deposited porous carbon electrode for supercapacitor, Electrochim. Acta 48 (2003) 641.
[27] C.C. Hu, W.Y. Li, J.Y. Lin, The capacitive characteristics of supercapacitors consisting of activated carbon fabric-polyaniline composites in NaNO3, J. Power Sources 137 (2004) 152.

[28] C. Tran, R. Singhal, D. Lawrence, V. Kalra, Polyaniline-coated freestanding porous carbon nanofibers as efficient hybrid electrodes for supercapacitors, J. Power Sources 293 (2015) 373.
[29] A. Olad, H. Gharekhani, Preparation and electrochemical investigation of the polyaniline/activated carbon nanocomposite for supercapacitor applications, Prog. Org. Coat. 81 (2015) 19.
[30] Y.N. Xia, J.M. Wiesinger, A.G. Macdiarmid, A.J. Epstein, Camphorsulfonic acid fully doped polyaniline emeraldine salt - conformations in different solvents studied by an ultraviolet-visible near-infrared spectroscopic method, Chem. Mat. 7 (1995) 443.
[31] H.B. Zhang, J.X. Wang, Z. Wang, F.B. Zhang, S.C. Wang, Electrodeposition of polyaniline nanostructures: A lamellar structure, Synth. Met. 159 (2009) 277.
[32] S.L. Mu, Y.F. Yang, Spectral characteristics of polyaniline nanostructures synthesized by using cyclic voltammetry at different scan rates, J. Phys. Chem. B 112 (2008) 11558.
[33] S. Mondal, K. Barai, N. Munichandraiah, High capacitance properties of polyaniline by electrochemical deposition on a porous carbon substrate, Electrochim. Acta 52 (2007) 3258.
[34] X.N. Chen, F.C. Meng, Z.W. Zhou, X. Tian, L.M. Shan, S.B. Zhu, X.L. Xu, M. Jiang, L. Wang, D. Hui, Y. Wang, J. Lu, J.H. Gou, One-step synthesis of graphene/polyaniline hybrids by in situ intercalation polymerization and their electromagnetic properties, Nanoscale 6 (2014) 8140.
[35] A. Janosevic, G. Ciric-Marjanovic, B. Marjanovic, P. Holler, M. Trchova, J. Stejskal, Synthesis and characterization of conducting polyaniline 5-sulfosalicylate nanotubes, Nanotechnology 19 (2008) 1.
[36] S.H. Tang, L.P. Sui, Z. Dai, Z.T. Zhu, H.X. Huangfu, High supercapacitive performance of Ni(OH)(2)/XC-72 composite prepared by microwave-assisted method, RSC Adv. 5 (2015) 43164.
[37] M. Mitra, C. Kulsi, K. Chatterjee, K. Kargupta, S. Ganguly, D. Banerjee, S. Goswamid, Reduced graphene oxide-polyaniline composites-synthesis, characterization and optimization for thermoelectric applications, RSC Adv. 5 (2015) 31039.
[38] L. Shi, R.P. Liang, J.D. Qiu, Controllable deposition of platinum nanoparticles on polyaniline-functionalized carbon nanotubes, J. Mater. Chem. 22 (2012) 17196.
[39] C. Dhand, M. Das, G. Sumana, A.K. Srivastava, M.K. Pandey, C.G. Kim, M. Datta, B.D. Malhotra, Preparation, characterization and application of polyaniline nanospheres to biosensing, Nanoscale 2 (2010) 747.
[40] L. Shi, R.-P. Liang, J.-D. Qiu, Controllable deposition of platinum nanoparticles on polyaniline-functionalized carbon nanotubes, J. Mater. Chem. 22 (2012) 17196.
[41] G. Wu, L. Li, J.H. Li, B.Q. Xu, Polyaniline-carbon composite films as supports of Pt and PtRu particles for methanol electrooxidation, Carbon 43 (2005) 2579.
[42] C.C. Hu, J.Y. Lin, Effects of the loading and polymerization temperature on the capacitive performance of polyaniline in NaNO3, Electrochim. Acta 47 (2002) 4055.
[43] L. Wang, Y.J. Ye, X.P. Lu, Z.B. Wen, Z. Li, H.Q. Hou, Y.H. Song, Hierarchical Nanocomposites of Polyaniline Nanowire Arrays on Reduced Graphene Oxide Sheets for Supercapacitors, Sci Rep 3 (2013) 1.
[44] R. Mazeikiene, A. Malinauskas, Electrochemical stability of polyaniline, Eur. Polym. J. 38 (2002) 1947.
[45] F. Béguin, V. Presser, A. Balducci, E. Frackowiak, Carbons and electrolytes for advanced supercapacitors, Adv. Mater. 26 (2014) 2219.
[46] B.L. Liang, Z.Y. Qin, T. Li, Z.J. Dou, F.X. Zeng, Y.M. Cai, M.F. Zhu, Z. Zhou, Poly(aniline-co-pyrrole) on the surface of reduced graphene oxide as high-performance electrode materials for supercapacitors, Electrochim. Acta 177 (2015) 335.
[47] M.K. Liu, Y.E. Miao, C. Zhang, W.W. Tjiu, Z.B. Yang, H.S. Peng, T.X. Liu, Hierarchical composites of polyaniline-graphene nanoribbons-carbon nanotubes as electrode materials in all-solid-state supercapacitors, Nanoscale 5 (2013) 7312.
[48] Q. Wu, Y.X. Xu, Z.Y. Yao, A.R. Liu, G.Q. Shi, Supercapacitors Based on Flexible Graphene/Polyaniline Nanofiber Composite Films, ACS Nano 4 (2010) 1963.

[49] C.H. Chang, T.C. Huang, C.W. Peng, T.C. Yeh, H.I. Lu, W.I. Hung, C.J. Weng, T.I. Yang, J.M. Yeh, Novel anticorrosion coatings prepared from polyaniline/graphene composites, Carbon 50 (2012) 5044.
[50] G.C. Li, G.R. Li, S.H. Ye, X.P. Gao, A Polyaniline-Coated Sulfur/Carbon Composite with an Enhanced High-Rate Capability as a Cathode Material for Lithium/Sulfur Batteries, Adv. Energy Mater. 2 (2012) 1238.
[51] C.J. Yan, L. Zou, R. Short, Single-walled carbon nanotubes and polyaniline composites for capacitive deionization, Desalination 290 (2012) 125.

## List of Figures in manuscript:

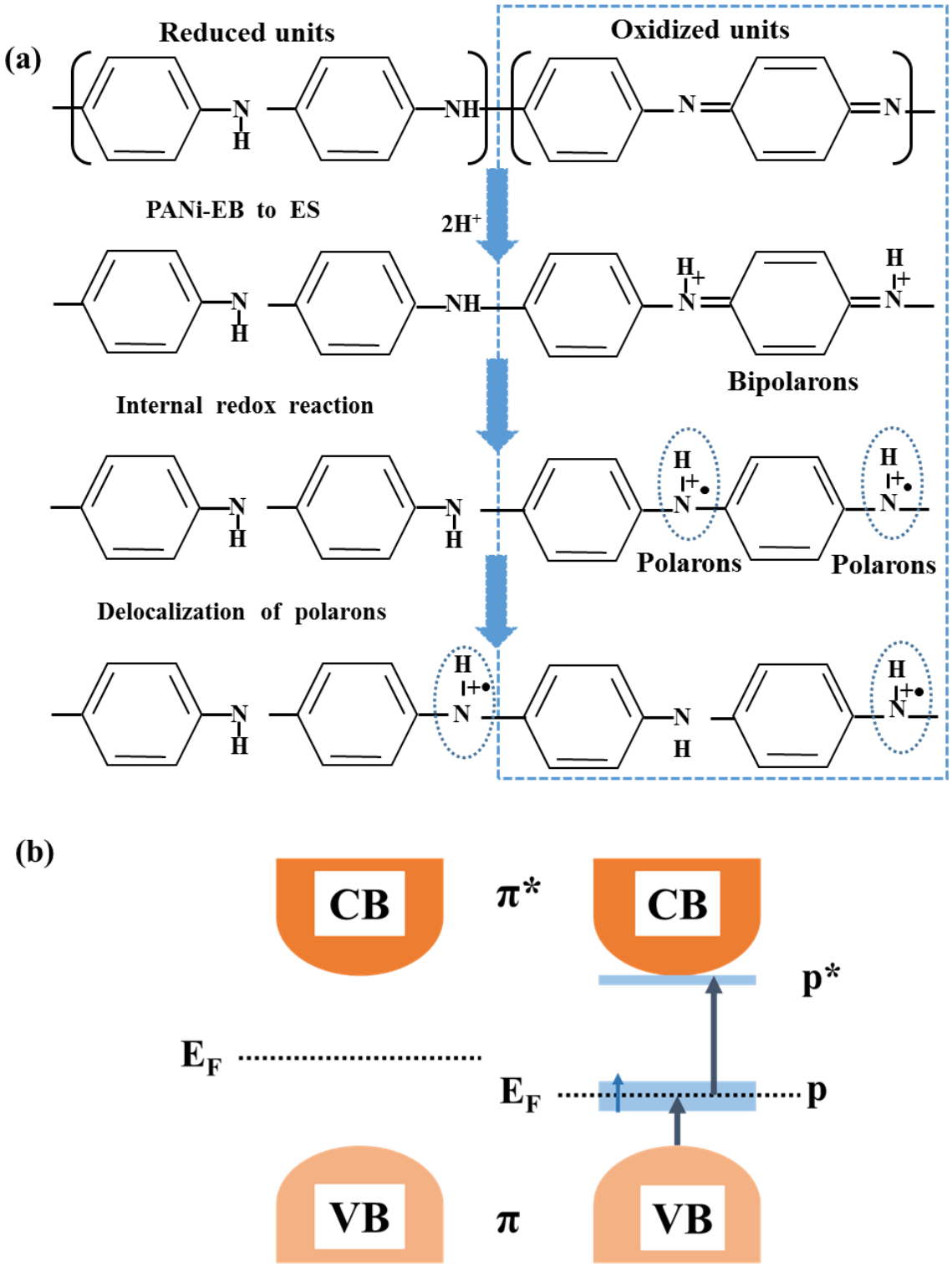


**Fig. 1.** (a) The polaron formation and conversion in PANi-ES. (b) the schematic energy band structure of PANi-ES with asymmetric upper (p*) and lower polaron bands (p). CB (π*) and VB (π) represent of conduction band and valence band, respectively.

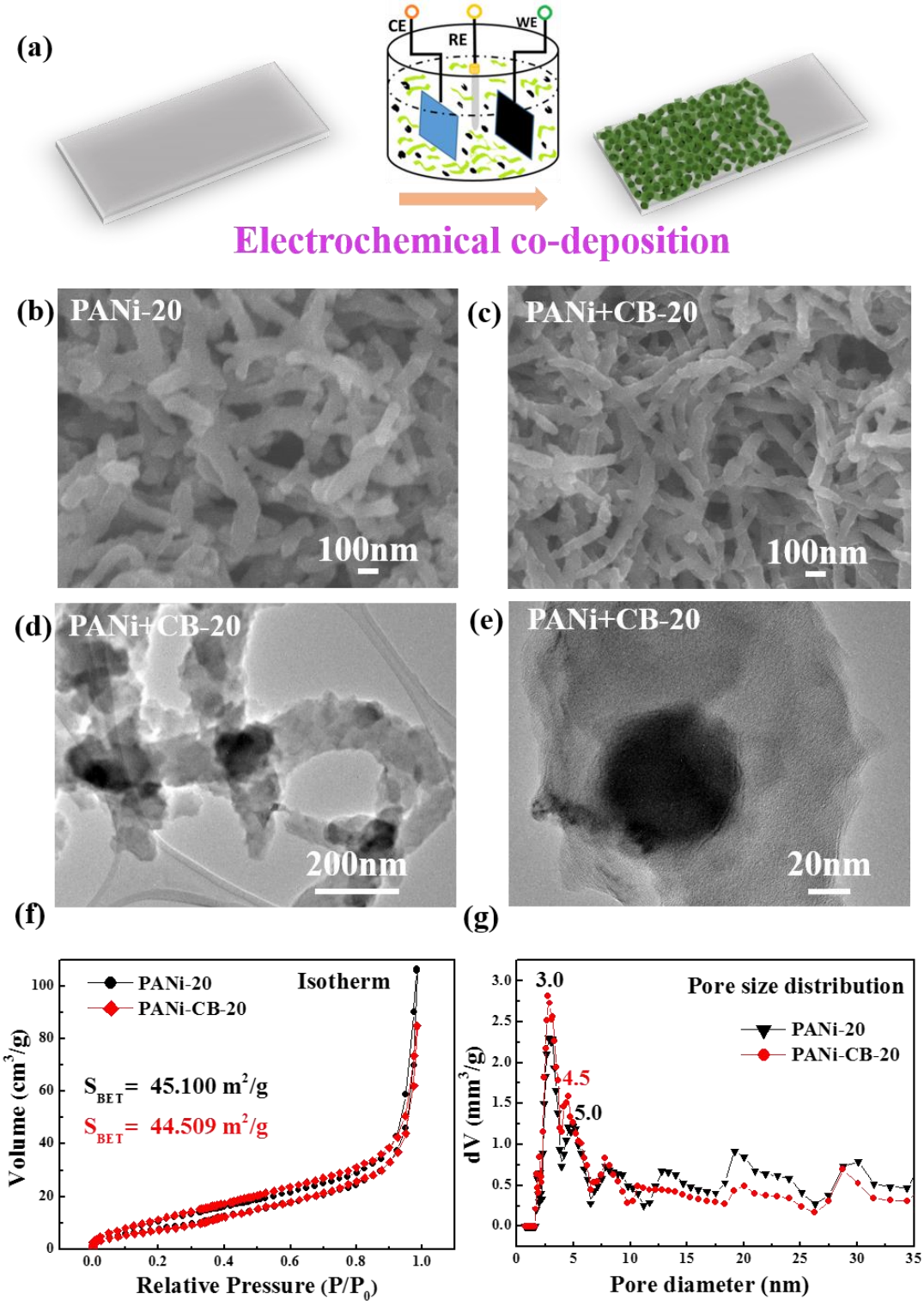


**Fig. 2.** (a) Schematic illustration of the synthesis of PANi based samples deposited on the GP substrate (left). After electrochemical co-deposition (middle), PANi/CB nanofibers are coated on the GP substrate (right). (b), (c) FE-SEM images of PANi-20 and PANi+CB-20, respectively. (d), (e) TEM images of PANi+CB-20 at low and high magnification. (f), (g) The $N_2$ adsorption/desorption isotherms and pore size distribution (PSD) curves of PANi-20 and PANi+CB-20.

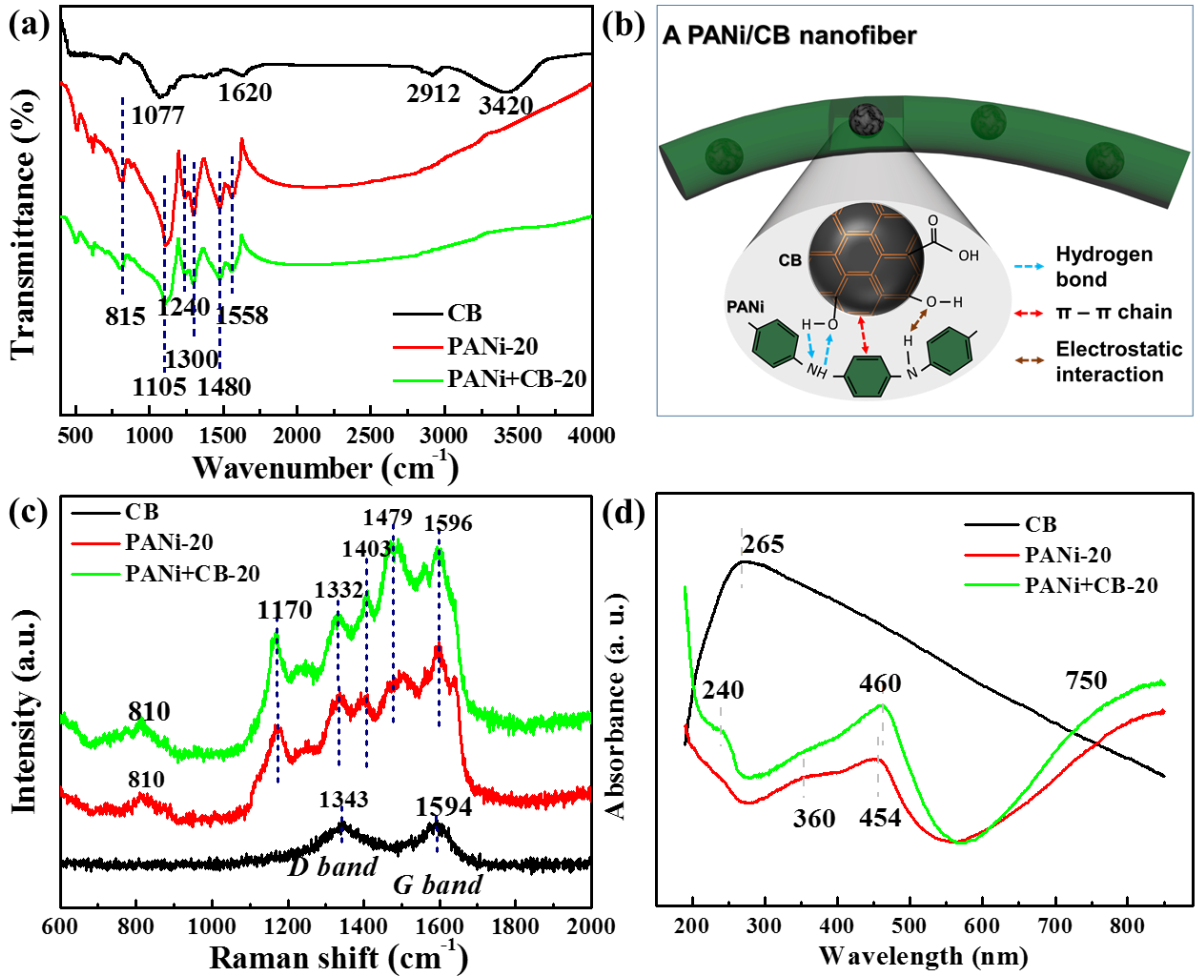


**Fig. 3.** (a) FTIR spectra of CB, PANi-20 and PANi+CB-20. (b) The schematic representation of the formation mechanism of PANi/CB composite. (c) Raman spectra of CB, PANi and PANi/CB electrodeposited on GP. (d) UV-visible spectra of PANi-20 and PANi+CB-20 deposited on Graphite paper.

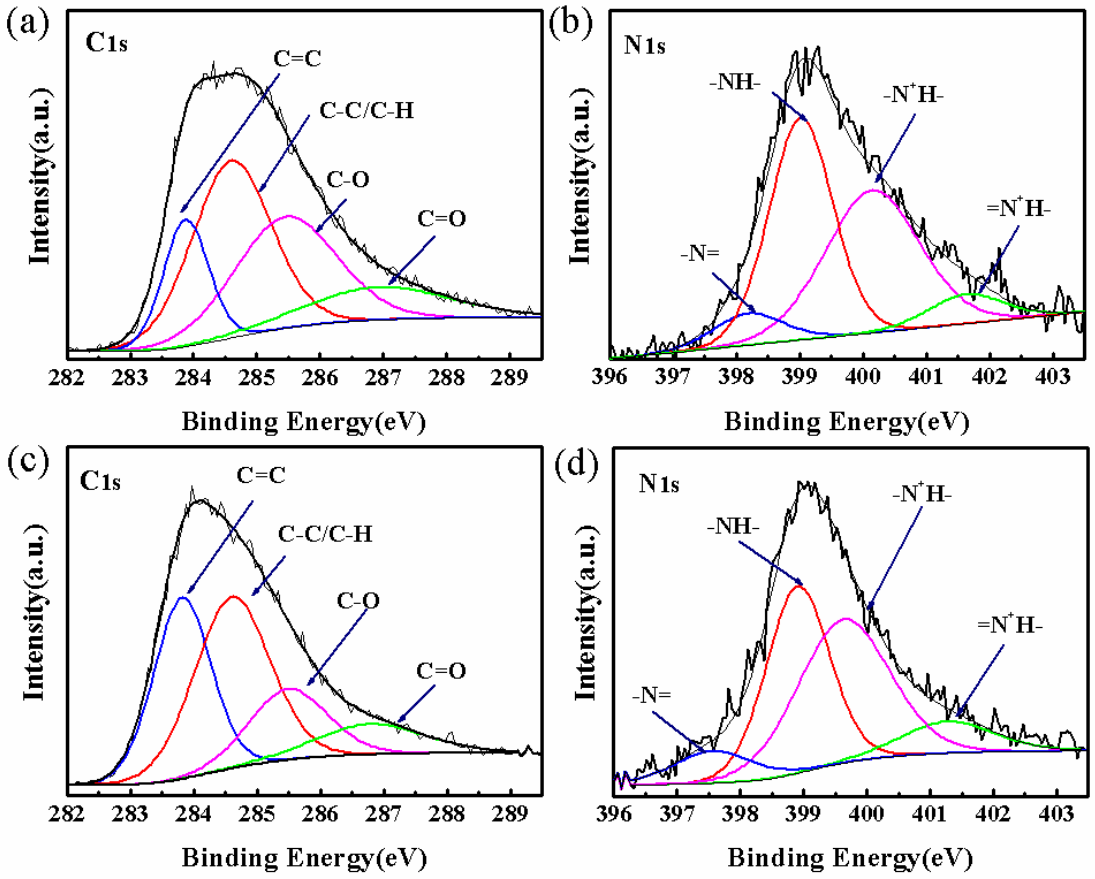


**Fig. 4.** C 1s regions of (a) PANi-20 and (c) PANi+CB-20. N 1s regions of (b) PANi-20 and (d) PANi+CB-20, respectively.

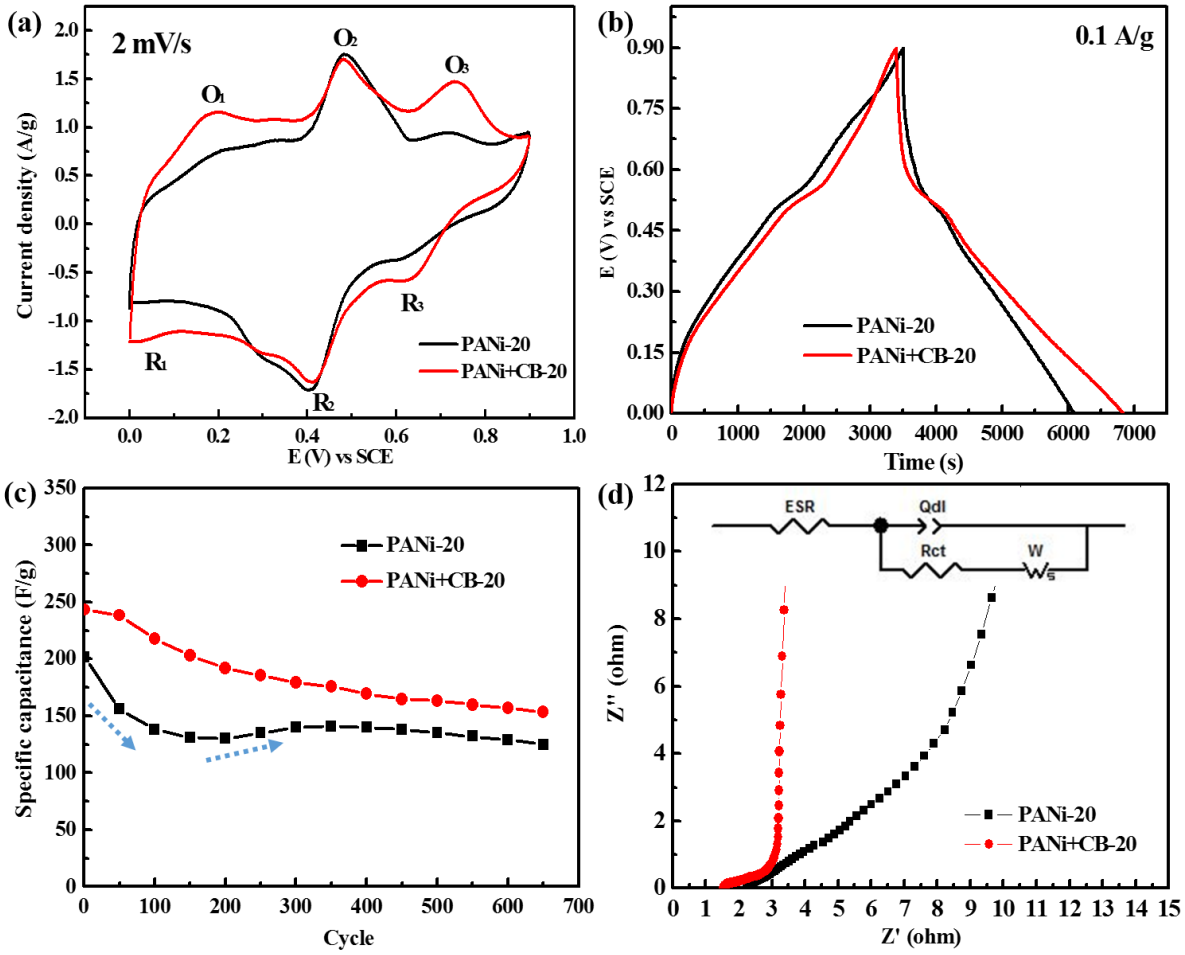


**Fig.5.** (a) CV curves at a scan rate of 2 mV $s^{-1}$ and (b) galvanostatic charge and discharge curves obtained at 0.1 A $g^{-1}$. (c) Cycling stability at a scan rate of 20 mV $s^{-1}$ for PANi-20 and PANi+CB-20. (d) Nyquist plots for PANi-20 and PANi+CB-20. The inset is the equivalent circuit used for impedance spectra fitting. Rel is the equivalent series resistance (ESR), Qdl is the element related with double layer capacitance, Rct is the charge transfer resistance and W is Warburg impedance.